Electrohydrodynamic interaction of spherical particles under Quincke rotation

Debasish Das and David Saintillan[*]

Department of Mechanical Science and Engineering, University of Illinois at Urbana-Champaign, Urbana, Illinois 61801, USA

Weakly conducting dielectric particles suspended in a dielectric liquid of higher conductivity can undergo a transition to spontaneous sustained rotation when placed in a sufficiently strong dc electric field. This phenomenon of Quincke rotation has interesting implications for the rheology of these suspensions, whose effective viscosity can be controlled and reduced by application of an external field. While previous models based on the rotation of isolated particles have provided accurate estimates for this viscosity reduction in dilute suspensions, discrepancies have been reported in more concentrated systems where particle-particle interactions are likely significant. Motivated by this observation, we extend the classic description of Quincke rotation based on the Taylor-Melcher leaky dielectric model to account for pair electrohydrodynamic interactions between two identical spheres using the method of reflections. A coupled system of evolution equations for the dipole moments and angular velocities of the spheres is derived that accounts for electric dipole-dipole interactions and hydrodynamic rotlet interactions up to order $O(R^{-5})$, where R is the separation distance between the spheres. A linear stability analysis of this system shows that interactions modify the value of the critical electric field for the onset of Quincke rotation: both electric and hydrodynamic interactions can either stabilize or destabilize the system depending on the orientation of the spheres, but the leading effect of interactions on the onset of rotation is hydrodynamic. We also analyze the dynamics in the nonlinear regime by performing numerical simulations of the governing equations. In the case of a pair of spheres that are fixed in space, we find that particle rotations always synchronize in magnitude at long times, though the directions of rotation of the spheres need not be the same. The steady-state angular velocity magnitude depends on the configuration of the spheres and electric field strength and agrees very well with an asymptotic estimate derived for corotating spheres. In the case of freely-suspended spheres, dipolar interactions are observed to lead to a number of distinct behaviors depending on the initial relative configuration of the spheres and on any infinitesimal initial perturbation introduced in the system: in some cases the spheres slowly separate in space while steadily rotating, while in other cases they pair up and either corotate or counterrotate depending on their orientation relative to the field.

PACS number(s): 47.65.−d, 83.80.Gv, 77.22.−d, 47.57.E−

I. INTRODUCTION

Electrorheological (ER) fluids, or collections of fine dielectric particles suspended in a dielectric liquid [1–4], are commonly used in a wide range of technological applications such as hydraulic valves [5] and clutches, brakes [6], shock absorbers [7], as well as in various microfluidic devices [8–10]. When placed in an electric field, the particles in an ER fluid polarize and interact, causing them in most cases to form chains and larger aggregation patterns in the direction of the field [1,11–14], thereby strongly enhancing the effective viscosity of the suspension. The formation of these internal structures is reversible and can be suppressed upon switching off of the field, offering an easy way of controlling the rheological properties of the fluid in real time. This so-called positive ER effect, by which chaining in the field direction results in a viscosity increase, is generally observed when the conductivity σ_2 of the suspended particles is larger than that of the carrier liquid, denoted by σ_1. The situation is quite different when $\sigma_1 > \sigma_2$, where chains and sheets of particles have been reported to form in directions perpendicular to the electric field and can result in an effective decrease in the apparent viscosity of the suspension [15].

Under certain conditions, application of a steady uniform electric field can also drive the spontaneous rotation of

spherical particles. This peculiar phenomenon was first discovered by Weiler [16] and Quincke [17] in the late nineteenth century, and has later become known as Quincke rotation. Detailed models for this effect were subsequently developed by Cebers [18] and Jones [19], who used Melcher and Taylor's leaky dielectric model [20,21] and identified the following mechanism for Quincke rotation. As depicted in Fig. 1, the sign of the dipole induced in a spherical particle placed in a uniform electric field depends on the properties of the particle and liquid phases. If the ratio of the dielectric permittivity to the conductivity of the material is larger in the suspending liquid than inside the particle, the induced dipole is parallel to the direction of the applied field; if it is less, the induced dipole is antiparallel. This ratio $\tau = \varepsilon/\sigma$ also corresponds to the characteristic relaxation time for the surface charge distribution on the surface of the particle upon application of the field. If the orientation of the sphere is weakly perturbed, a mechanical torque arises as a result of the Maxwell stress in the fluid, which is restoring in the first case but destabilizing in the second case. If the electric field is strong enough to overcome the effect of the viscous torque on the particle, this can result in the steady spontaneous rotation of the particle with a constant angular velocity around an arbitrary axis perpendicular to the direction of the applied field. To summarize, Quincke rotation occurs if

$$\frac{\varepsilon_2}{\sigma_2} > \frac{\varepsilon_1}{\sigma_1}, \tag{1}$$
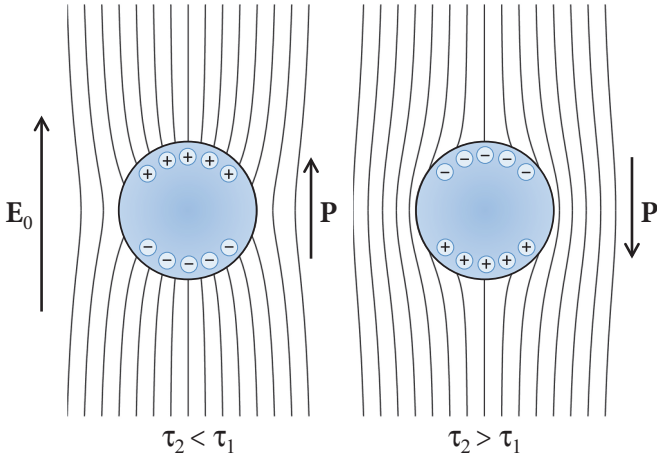
---
[*]dstn@illinois.edu

FIG. 1. (Color online) Polarization of a spherical particle in an applied electric field $\mathbf{E}_0$. (Left) If the charge relaxation time $\tau_2 = \varepsilon_2/\sigma_2$ of the particle is less than that, $\tau_1 = \varepsilon_1/\sigma_1$, of the suspending fluid, the induced dipole $\mathbf{P}$ is parallel to the applied field; (right) if it is greater, the induced dipole is antiparallel (after Ref. [19]).

which is to say that the characteristic charge relaxation time is larger inside the particle than outside, and if the electric field strength exceeds a critical value E_c whose expression will be derived in Sec. II A in terms of material properties. A full stability analysis of the dynamical system shows that the onset of Quincke rotation is associated with a supercritical pitchfork bifurcation. If particle inertia is significant, the dynamics of the system are formally identical to those of the classic Lorenz oscillator [22], and further increasing the field strength therefore eventually leads to a second bifurcation to unsteady chaotic dynamics [23], as has also been observed in experiments [24]. Spontaneous electrorotation followed by complex deformation dynamics has also been reported in experiments on weakly conducting droplets suspended in a less conducting fluid when placed in a strong electric field [25–28].

Quincke electrorotation in large-scale suspensions has interesting consequences for the effective rheology of the suspensions [29–35]. When an external shear flow is applied (for instance in a Couette device or in pressure-driven Poiseuille flow) together with a sufficiently strong external electric field in the flow gradient direction, Quincke rotation arises in the same direction as the external flow vorticity and thereby effectively decreases the apparent viscosity of the suspension. This effect, which is easy to interpret theoretically [34,36,37], has been observed in a number of experiments in both Couette and pressure-driven flow setups [29–33]. An increase in the effective electric conductivity of the suspension has also been observed [38,39]. While experiments show fairly good agreement with simple dilute theoretical predictions for the change in viscosity in sufficiently strong flows of dilute suspensions [30], departures from these predictions have been reported at low shear rates and high concentrations, presumably as a result of particle-particle electrohydrodynamic interactions, which may cause structuring of the suspension in the form of chains or other types of aggregates as in previously studied ER fluids.

Particle-particle interactions in Quincke rotation have only received limited attention up to now, in part owing to the strongly nonlinear nature of the governing set of equations,

which will be described below. In early work, Wan *et al.* [40] considered the electrostatic interaction of a pair of dielectric spheres, and derived the induced dipoles in both spheres using bispherical coordinates. They then used this result to evaluate the mean force on a particle when one of the two spheres was rotated at a constant angular velocity around the other one. Their study, however, did not account for the change in polarization of the particles as a result of Quincke rotation nor for the effect of hydrodynamic interactions. More recently, a significantly more detailed analysis was proposed by Dolinsky and Elperin [41], who used a somewhat similar treatment as in the present work. They applied the method of reflections to analyze Quincke rotation of a pair of spheres in an external field. They derived expressions for the induced electric dipoles in both spheres that accounted for electric interactions as well as particle rotations, and used these expressions to draw conclusions on the effect of interactions on the angular velocity of the spheres and electric forces due to dipole-dipole interactions. Their study, however, entirely neglected hydrodynamic interactions due to the rotation and motion of the spheres; these interactions, as we show below, are as important as electric interactions as they modify the induced dipoles and resulting angular velocities at the same asymptotic order.

In the present paper, we describe a detailed asymptotic analysis of the effects of both electric and hydrodynamic interactions on Quincke rotation of a pair of identical spheres suspended in an unbounded domain when a uniform external electric field is applied. The details of the model, which is based on the leaky dielectric model of Melcher and Taylor [20] and extends previous classic studies of Quincke rotation of isolated particles [18,19], are presented in Sec. II, where a set of coupled nonlinear ordinary differential equations for the dipole moments and angular velocities of the two spheres are derived using the method of reflections [42] and are valid to order $O(R^{-5})$, where R denotes the distance between the two spheres. This set of equations is then used to study the stability of the system in Sec. III, where a linear stability analysis shows that interactions can either increase or decrease the value of the critical electric field for onset of rotation depending on the configuration of the spheres. Finally, we also carry out numerical simulations of both fixed and freely suspended spheres in Sec. IV, and show that interactions lead to synchronization of the particle rotations and either pairing or separation of the two particles depending on their initial configuration and on the infinitesimal perturbation introduced in the system at $t = 0$. We conclude in Sec. V.

II. THEORETICAL MODEL

A. Single sphere in a nonuniform field

1. Governing equations and moment equations

We first analyze in detail the case of a single isolated sphere of radius a placed in an infinite liquid and subject to a nonuniform external electric field $\mathbf{E}_e(\mathbf{x}) = -\nabla\phi_e(\mathbf{x})$ as depicted in Fig. 2. Denote by $(\varepsilon_1, \sigma_1)$ the permittivity and conductivity of the suspending liquid, and by $(\varepsilon_2, \sigma_2)$ those of the particle. We adopt a coordinate system with the origin at the center of the sphere, and we assume that the external
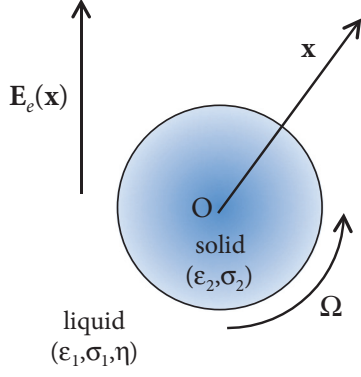
FIG. 2. (Color online) Isolated sphere undergoing Quincke rotation in a nonuniform external field $\mathbf{E}_e(\mathbf{x})$.

potential $\phi_e(\mathbf{x})$ in the absence of the sphere can be expanded in a Taylor series about the origin as

$$\phi_e(\mathbf{x}) = \phi_e(\mathbf{0}) + \mathbf{x} \cdot \nabla \phi_e(\mathbf{0}) + \tfrac{1}{2}\mathbf{xx} : \nabla\nabla\phi_e(\mathbf{0}) + \cdots, \quad (2)$$

where we neglect higher-order terms in this discussion for reasons that will become clear in Sec. II B. The presence of the sphere perturbs the external potential as

$$\phi(\mathbf{x}) = \begin{cases} \phi^+(\mathbf{x}) = \phi_e(\mathbf{x}) + \phi_d^+(\mathbf{x}) & \text{if } |\mathbf{x}| > a, \\ \phi^-(\mathbf{x}) = \phi_e(\mathbf{x}) + \phi_d^-(\mathbf{x}) & \text{if } |\mathbf{x}| < a, \end{cases} \quad (3)$$

where we wish to determine the disturbance potentials $\phi_d^+(\mathbf{x})$ and $\phi_d^-(\mathbf{x})$ outside and inside the sphere, respectively.

Following the classic Taylor-Melcher leaky dielectric model [20,21], which was also used in previous studies of Quincke rotation [18,19], we assume that any induced charge in the system is concentrated at the interface between the solid and liquid in the form of a surface charge distribution $q(\mathbf{x})$, which is related to the normal jump in the electric displacement field across the interface via Gauss's law [43],

$$q(\mathbf{x}) = \mathbf{n} \cdot [\![\varepsilon\mathbf{E}(\mathbf{x})]\!] = -\mathbf{n} \cdot [\varepsilon_1\nabla\phi^+(\mathbf{x}) - \varepsilon_2\nabla\phi^-(\mathbf{x})], \quad (4)$$

where $\mathbf{n} = \mathbf{x}/x$ is a unit outward normal on the particle surface. Under this assumption, both disturbance potentials satisfy Laplace's equation since there is no net charge in the solid and liquid away from the interface

$$\nabla^2\phi_d^+(\mathbf{x}) = \nabla^2\phi_d^-(\mathbf{x}) = 0. \quad (5)$$

This will allow us to seek solutions as expansions in spherical harmonics below. Boundary conditions on the potentials are as follows. First, the disturbance potential outside the sphere must decay far away from the surface:

$$\phi_d^+(\mathbf{x}) \to 0 \quad \text{as } |\mathbf{x}| \to \infty. \quad (6)$$

Second, the potential must be continuous across the interface:

$$\phi_d^+(\mathbf{x}) = \phi_d^-(\mathbf{x}) \quad \text{if } |\mathbf{x}| = a. \quad (7)$$

The third boundary condition expresses charge conservation on the interface as a result of Ohmic currents from the bulk and charge convection by the moving surface:

$$\frac{\partial q}{\partial t} + \mathbf{n} \cdot [\![\mathbf{J}]\!] + \nabla_s \cdot (q\mathbf{V}) = 0 \quad \text{at } |\mathbf{x}| = a. \quad (8)$$

In Eq. (8), $\mathbf{n} \cdot [\![\mathbf{J}]\!]$ denotes the normal jump in Ohmic current across the interface:

$$\mathbf{n} \cdot [\![\mathbf{J}(\mathbf{x})]\!] = \mathbf{n} \cdot [\![\sigma\mathbf{E}(\mathbf{x})]\!] = -\mathbf{n} \cdot [\sigma_1\nabla\phi^+(\mathbf{x}) - \sigma_2\nabla\phi^-(\mathbf{x})]. \quad (9)$$

Also, $\nabla_s = (\mathbf{I} - \mathbf{nn}) \cdot \nabla$ is the surface divergence operator, and $\mathbf{V}$ is the velocity of a point on the sphere surface, which is assumed to be rotating at a yet unknown angular velocity $\mathbf{\Omega}$: $\mathbf{V} = \mathbf{\Omega} \times a\mathbf{n}$.

Solutions of Eq. (5) for the disturbance potentials outside and inside the sphere can be written as expansions in decaying and growing spherical harmonics, respectively,

$$\phi_d^+(\mathbf{x}) = \frac{\mathbf{x} \cdot \mathbf{P}}{x^3} + \frac{1}{2}\frac{\mathbf{xx} : \mathbf{Q}}{x^5} + \cdots, \quad (10)$$

$$\phi_d^-(\mathbf{x}) = \frac{\mathbf{x} \cdot \mathbf{P}}{a^3} + \frac{1}{2}\frac{\mathbf{xx} : \mathbf{Q}}{a^5} + \cdots, \quad (11)$$

which automatically satisfy the two boundary conditions of Eqs. (6) and (7). In Eqs. (10) and (11), vector $\mathbf{P}$ denotes the dipole moment on the sphere, and second-order tensor $\mathbf{Q}$ denotes the quadrupole moment. We do not include any monopole in the expansions as the sphere is assumed to carry no net charge. Higher-order multipoles could also be included, though we will not consider them here as these will be negligible in the study of pair interactions in Sec. II B. Substituting these expansions into the charge conservation equation (8) allows one to derive evolution equations for the moments $\mathbf{P}$ and $\mathbf{Q}$ as

$$\frac{d\mathbf{P}}{dt} = \mathbf{\Omega} \times [\mathbf{P} + a^3\varepsilon_{21}\nabla\phi_e(\mathbf{0})] - \frac{1}{\tau_{\text{MW}}}[\mathbf{P} + a^3\sigma_{21}\nabla\phi_e(\mathbf{0})], \quad (12)$$

$$\frac{d\mathbf{Q}}{dt} = \mathbf{\Omega} \times [\mathbf{Q} + a^5\varepsilon_{21}'\nabla\nabla\phi_e(\mathbf{0})] - \frac{1}{\tau_{\text{MW}}'}[\mathbf{Q} + a^5\sigma_{21}'\nabla\nabla\phi_e(\mathbf{0})], \quad (13)$$

where τ_{MW} and τ_{MW}' are the first and second Maxwell-Wagner relaxation times,

$$\tau_{\text{MW}} = \frac{\varepsilon_2 + 2\varepsilon_1}{\sigma_2 + 2\sigma_1}, \quad \tau_{\text{MW}}' = \frac{2\varepsilon_2 + 3\varepsilon_1}{2\sigma_2 + 3\sigma_1}, \quad (14)$$

and where we have introduced the following dimensionless parameters:

$$\varepsilon_{21} = \frac{\varepsilon_2 - \varepsilon_1}{\varepsilon_2 + 2\varepsilon_1}, \quad \varepsilon_{21}' = \frac{\varepsilon_2 - \varepsilon_1}{2\varepsilon_2 + 3\varepsilon_1},$$
$$\sigma_{21} = \frac{\sigma_2 - \sigma_1}{\sigma_2 + 2\sigma_1}, \quad \sigma_{21}' = \frac{\sigma_2 - \sigma_1}{2\sigma_2 + 3\sigma_1}. \quad (15)$$

In Eq. (13), the notations $\mathbf{\Omega} \times \mathbf{Q}$ and $\mathbf{\Omega} \times \nabla\nabla\phi_e(\mathbf{0})$ are used to denote the following two tensors in index notation:

$$[\mathbf{\Omega} \times \mathbf{Q}]_{ij} = \epsilon_{ikl}\Omega_k Q_{lj},$$
$$[\mathbf{\Omega} \times \nabla\nabla\phi_e(\mathbf{0})]_{ij} = \epsilon_{ikl}\Omega_k\frac{\partial^2\phi_e}{\partial x_l \partial x_j}(\mathbf{0}). \quad (16)$$

Equation (12) for the dipole moment $\mathbf{P}$ differs slightly from the dipole evolution equation appearing in previous studies of Quincke rotation [34,35], through the presence of the term involving $\mathbf{\Omega} \times \nabla\phi_e(\mathbf{0})$. This discrepancy is easily resolved

by realizing that the dipole **P** appearing in Eq. (12) is the total dipole moment on the particle, whereas previous studies have typically focused on the retarding dipole moment defined as $\mathbf{P}_r = \mathbf{P} - \mathbf{P}_\infty$, where $\mathbf{P}_\infty = -a^3 \varepsilon_{21} \nabla \phi_e(\mathbf{0})$ is the instantaneous polarization. From Eq. (12), it is straightforward to recover the commonly used equation for $\mathbf{P}_r$

$$\frac{d\mathbf{P}_r}{dt} = \mathbf{\Omega} \times \mathbf{P}_r - \frac{1}{\tau_{\mathrm{MW}}} [\mathbf{P}_r - a^3 (\varepsilon_{21} - \sigma_{21}) \nabla \phi_e(\mathbf{0})]. \quad (17)$$

Similarly, an equation can be written for the retarding quadrupole moment $\mathbf{Q}_r = \mathbf{Q} - \mathbf{Q}_\infty$ where $\mathbf{Q}_\infty = -a^5 \varepsilon'_{21} \nabla \nabla \phi_e(\mathbf{0})$ as

$$\frac{d\mathbf{Q}_r}{dt} = \mathbf{\Omega} \times \mathbf{Q}_r - \frac{1}{\tau'_{\mathrm{MW}}} [\mathbf{Q}_r - a^5 (\varepsilon'_{21} - \sigma'_{21}) \nabla \nabla \phi_e(\mathbf{0})]. \quad (18)$$

For the purpose of studying Quincke rotation, it is equivalent to use $(\mathbf{P}, \mathbf{Q})$ or $(\mathbf{P}_r, \mathbf{Q}_r)$, as we will see below that the instantaneous dipole and quadrupole moments $\mathbf{P}_\infty$ and $\mathbf{Q}_\infty$ do not contribute to the electric torque on the particle. In this work, we make the choice of working with the total moments **P** and **Q**, which satisfy Eqs. (12) and (13). The physical interpretation of Eqs. (12) and (13) is straightforward: the retarding parts of the dipole and quadrupole moments are subject to the rotation of the particle with angular velocity **Ω**, while the total dipole and quadrupole simultaneously relax toward their steady-state values in the absence of rotation. The time scales for these relaxation processes are given by the Maxwell-Wagner relaxation times of Eq. (14). It is also easy to see how additional equations for higher multipole moments could be obtained, though we do not include them here. It should be noted that the set of uncoupled equations (12) and (13) for the multipolar moments is a direct consequence of the leaky dielectric model and in particular of the boundary condition of Eq. (8) for the surface charge conservation; more sophisticated statistical mechanical models for dielectric relaxation based on a Fokker-Planck equation for the probability distribution of noninteracting polar molecules have suggested that a coupling between multipolar moments may in fact exist [44,45], though we do not include it here.

2. Balance of angular momentum

In the above discussion, we have assumed that the sphere is rotating at a given angular velocity **Ω**, which is still unknown. To determine **Ω**, we write down the angular momentum balance for the sphere, which is subject to both viscous and electric torques,

$$I \frac{d\mathbf{\Omega}}{dt} = -8\pi \eta a^3 \mathbf{\Omega} + \mathbf{T}^e. \quad (19)$$

Here, $I = 2ma^3/5$ is the moment of inertia of a sphere of mass m, η is the viscosity of the suspending liquid, and $\mathbf{T}^e$ is the electric torque on the particle. Both the dipole and quadrupole moments can contribute to the electric torque, which was previously calculated by Jones and Washizu [46] as

$$\mathbf{T}^e = -4\pi \varepsilon_1 [\mathbf{P} \times \nabla \phi_e(\mathbf{0}) + (\mathbf{Q} \cdot \nabla) \times \nabla \phi_e(\mathbf{0})], \quad (20)$$

or, in index notation,

$$T_i^e = -4\pi \varepsilon_1 \left[\epsilon_{ijk} P_j \frac{\partial \phi_e}{\partial x_k}(\mathbf{0}) + \epsilon_{ijk} Q_{jl} \frac{\partial^2 \phi_e}{\partial x_l \partial x_k}(\mathbf{0}) \right]. \quad (21)$$

From this expression, it is easy to see that the instantaneous dipole and quadrupole moments, which are collinear with $\nabla \phi_e(\mathbf{0})$ and $\nabla \nabla \phi_e(\mathbf{0})$, respectively, do not result in any torque on the particle.

In this paper, we focus on the inertialess limit where the left-hand side in Eq. (19) is negligible. In this case, the angular momentum balance simplifies to the following relation between angular velocity and multipole moments:

$$2\eta a^3 \mathbf{\Omega} + \varepsilon_1 [\mathbf{P} \times \nabla \phi_e(\mathbf{0}) + (\mathbf{Q} \cdot \nabla) \times \nabla \phi_e(\mathbf{0})] = 0. \quad (22)$$

Equations (12) and (13), together with Eq. (22), constitute a coupled system of equations for **P**, **Q**, and **Ω**, which can be analyzed or integrated numerically given an initial condition.

3. Steady-state solutions

We first seek steady-state solutions to this system of equations, with the aim of determining conditions for spontaneous steady rotation to arise. At steady state, Eqs. (12) and (13) for the dipole and quadrupole moments reduce to

$$\mathbf{\Omega} \times \mathbf{P} - \frac{1}{\tau_{\mathrm{MW}}} \mathbf{P} = \frac{a^3 \sigma_{21}}{\tau_{\mathrm{MW}}} \nabla \phi_e(\mathbf{0}) - a^3 \varepsilon_{21} \mathbf{\Omega} \times \nabla \phi_e(\mathbf{0}), \quad (23)$$

$$\mathbf{\Omega} \times \mathbf{Q} - \frac{1}{\tau'_{\mathrm{MW}}} \mathbf{Q} = \frac{a^3 \sigma'_{21}}{\tau'_{\mathrm{MW}}} \nabla \nabla \phi_e(\mathbf{0}) - a^3 \varepsilon'_{21} \mathbf{\Omega} \times \nabla \nabla \phi_e(\mathbf{0}). \quad (24)$$

These two equations admit analytical solutions for **P** and **Q**,

$$\mathbf{P} = A_1 [\mathbf{\Omega} \times \nabla \phi_e(\mathbf{0}) + \tau_{\mathrm{MW}} (\mathbf{\Omega} \cdot \nabla \phi_e(\mathbf{0})) \mathbf{\Omega}] - A_2 \nabla \phi_e(\mathbf{0}), \quad (25)$$

$$\mathbf{Q} = A_3 [\mathbf{\Omega} \times \nabla \nabla \phi_e(\mathbf{0}) + \tau'_{\mathrm{MW}} (\mathbf{\Omega} \cdot \nabla \nabla \phi_e(\mathbf{0})) \mathbf{\Omega}] - A_4 \nabla \nabla \phi_e(\mathbf{0}), \quad (26)$$

where the coefficients A_1 through A_4 are given by

$$A_1 = \frac{a^3 \tau_{\mathrm{MW}} (\varepsilon_{21} - \sigma_{21})}{1 + \Omega^2 \tau_{\mathrm{MW}}^2}, \quad A_2 = a^3 \left[\varepsilon_{21} + \frac{\sigma_{21} - \varepsilon_{21}}{1 + \Omega^2 \tau_{\mathrm{MW}}^2} \right], \quad (27)$$

$$A_3 = \frac{a^3 \tau'_{\mathrm{MW}} (\varepsilon'_{21} - \sigma'_{21})}{1 + \Omega^2 \tau'^2_{\mathrm{MW}}}, \quad A_4 = a^3 \left[\varepsilon'_{21} + \frac{\sigma'_{21} - \varepsilon'_{21}}{1 + \Omega^2 \tau'^2_{\mathrm{MW}}} \right]. \quad (28)$$

Finally, substituting Eqs. (25) and (26) into the torque balance Eq. (22) yields a nonlinear equation for the angular velocity **Ω**.

Obtaining an exact analytical expression for **Ω** or its norm when the electric field is nonuniform (i.e., when $\nabla \nabla \phi_e(\mathbf{0}) \neq \mathbf{0}$) is not straightforward, though Eq. (22) could still be used in numerical simulations. However, the case of a uniform field can be further analyzed. If $\nabla \nabla \phi_e(\mathbf{0}) = \mathbf{0}$ and $\mathbf{Q} = \mathbf{0}$, the equation for **Ω** simplifies to

$$2\eta a^3 \mathbf{\Omega} + \varepsilon_1 A_1 [\mathbf{\Omega} \times \nabla \phi_e + \tau_{\mathrm{MW}} (\mathbf{\Omega} \cdot \nabla \phi_e) \mathbf{\Omega}] \times \nabla \phi_e = \mathbf{0}. \quad (29)$$

Taking the dot product of Eq. (29) with the local potential gradient $\nabla \phi_e$ immediately yields

$$\mathbf{\Omega} \cdot \nabla \phi_e = 0, \quad (30)$$

i.e., any particle rotation will have an angular velocity $\mathbf{\Omega}$ normal to the direction of the external field. The exact direction of rotation is however indeterminate. The magnitude of the angular velocity can be obtained by taking the dot product of Eq. (29) with $\mathbf{\Omega}$

$$2\eta a^3 \Omega^2 - \varepsilon_1 A_1 \Omega^2 E_e^2 = 0, \tag{31}$$

where we have introduced the magnitude of the external electric field $\mathbf{E}_e = -\nabla \phi_e$. Using Eq. (27) for A_1, which is itself a function of Ω^2, we obtain a biquadratic equation for $\Omega = |\mathbf{\Omega}|$,

$$\Omega^2 \left[\Omega^2 \tau_{\text{MW}}^2 + 1 - \frac{\varepsilon_1 \tau_{\text{MW}}(\varepsilon_{21} - \sigma_{21})}{2\eta} E_e^2 \right] = 0. \tag{32}$$

The solution $\Omega = 0$ always exists and corresponds to the absence of rotation. However, another solution is also given by

$$\Omega = \pm \frac{1}{\tau_{\text{MW}}} \sqrt{\left(\frac{E_e}{E_c}\right)^2 - 1}, \quad \text{with}$$

$$E_c = \sqrt{\frac{2\eta}{\varepsilon_1 \tau_{\text{MW}}(\varepsilon_{21} - \sigma_{21})}}. \tag{33}$$

This solution, which is the same as that obtained in previous studies of Quincke rotation [19], only arises when the value of the external field E_e exceeds the critical value E_c. The solutions are plotted in Fig. 3, where we see that the steady solution with $\mathbf{\Omega} = \mathbf{0}$ bifurcates at $E_e = E_c$. From the definition of E_c, it is clear that Quincke rotation can only occur if $\varepsilon_{21} > \sigma_{21}$, which is easily shown to be equivalent to

$$\frac{\varepsilon_2}{\sigma_2} > \frac{\varepsilon_1}{\sigma_1}, \tag{34}$$

in agreement with the physical interpretation provided in Sec. I.

A linear stability analysis of the dynamical system shows that the onset of Quincke rotation corresponds to a supercritical pitchfork bifurcation, and that the steady solution loses its stability when $E_e > E_c$. In experiments, spontaneous rotation is expected to take place in this case, around an arbitrary
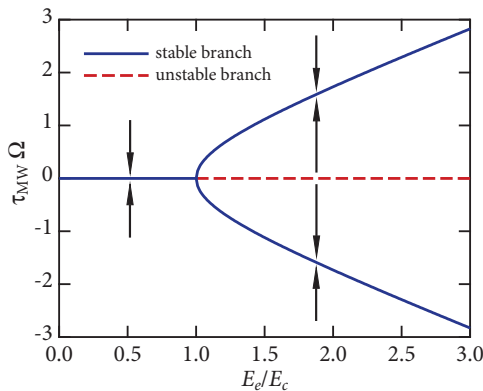
FIG. 3. (Color online) Stability diagram for the angular velocity magnitude of a single sphere. A supercritical pitchfork bifurcation occurs at $E_e = E_c$; above this value, the solution $\Omega = 0$ becomes unstable and spontaneous rotation occurs with an angular velocity given by Eq. (33).
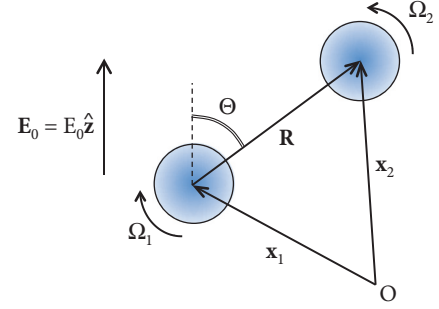
FIG. 4. (Color online) Interaction of two identical spheres undergoing Quincke rotation in a uniform field $\mathbf{E}_0$.

direction perpendicular to the field direction and with an angular velocity magnitude given by Eq. (33). In the absence of particle inertia, the two branches defined by Eq. (33) are stable for any field strength satisfying $E_e > E_c$. If inertia is retained in the angular momentum balance of Eq. (19), previous studies have shown that the governing equations for $\mathbf{P}$ and $\mathbf{\Omega}$ can be reduced to the Lorenz oscillator equations [22], and that a transition to chaos therefore occurs in very strong fields [23,24].

B. Two spheres in a uniform field

1. Electric problem

We now consider the case of two identical spheres separated by a vector $\mathbf{R} = \mathbf{x}_2 - \mathbf{x}_1$ and placed in a uniform electric field $\mathbf{E}_0$ as depicted in Fig. 4. We also define the notations $R = |\mathbf{R}|$ and $\widehat{\mathbf{R}} = \mathbf{R}/R$. We wish to analyze the leading-order effect of electric and hydrodynamic interactions between the spheres based on the single-particle results derived in Sec. II A and using the method of reflections. Note that because the spheres perturb the electric field around them, they really experience a nonuniform field as a result of interactions. First, each sphere polarizes under the field, and develops a dipole moment $\mathbf{P}_\alpha$ (with $\alpha = 1,2$) obtained by a generalization of the dipole relaxation equation (12). For sphere 1

$$\frac{d\mathbf{P}_1}{dt} = \mathbf{\Omega}_1 \times \left[\mathbf{P}_1 + a^3 \varepsilon_{21} \nabla \phi_e^1(\mathbf{x}_1) \right]$$
$$- \frac{1}{\tau_{\text{MW}}} \left[\mathbf{P}_1 + a^3 \sigma_{21} \nabla \phi_e^1(\mathbf{x}_1) \right], \tag{35}$$

and a similar equation can also be written for the dipole moment $\mathbf{P}_2$ of the second sphere. A relaxation equation based on Eq. (13) can also be written for the quadrupole moment $\mathbf{Q}_\alpha$ induced in each sphere, though we will show below that it can be neglected to leading order. In Eq. (35), $\nabla \phi_e^1(\mathbf{x}_1)$ denotes the external electric field (up to a minus sign) experienced by sphere 1. This electric field includes the applied uniform field $\mathbf{E}_0$, as well as a correction arising from the potential disturbance $\phi_d^{+2}(\mathbf{x})$ induced by the various multipoles generated inside sphere 2. To leading order, according to Eq. (10)

$$\phi_d^{+2}(\mathbf{x}) = \frac{(\mathbf{x} - \mathbf{x}_2) \cdot \mathbf{P}_2}{|\mathbf{x} - \mathbf{x}_2|^3} + \cdots, \tag{36}$$

which can be expanded on the basis of growing spherical harmonics near the center of sphere 1 to obtain the correction

to the applied field. All calculations done, the potential gradient $\nabla\phi_e^1(\mathbf{x}_1)$ appearing in Eq. (35) can be shown to be of the form

$$\nabla\phi_e^1(\mathbf{x}_1) = -\mathbf{E}_0 + \frac{1}{R^3}\mathbf{\Pi}\cdot\mathbf{P}_2 + O(R^{-8}), \qquad (37)$$

where we have introduced the second-order tensorial operator $\mathbf{\Pi} = \mathbf{I} - 3\widehat{\mathbf{R}}\widehat{\mathbf{R}}$. The error in Eq. (37), which arises from neglecting the contributions of the quadrupole moment and higher multipoles to the disturbance potential, can be estimated to be of order $O(R^{-8})$. Indeed, because the applied field is uniform, the leading-order quadrupole moment induced inside the spheres arises from the second gradient of the disturbance potential ϕ_d^+ resulting from the dipole moments and is therefore of order $|\mathbf{Q}_\alpha| = O(R^{-4})$ as can be seen from Eq. (36). The quadrupole moment then adds an $O(R^{-7})$ correction to the disturbance potential [see Eq. (10)], corresponding to an $O(R^{-8})$ correction to the potential gradient in Eq. (37).

2. Torque balance

To determine the angular velocity $\mathbf{\Omega}_1$ appearing in Eq. (35), we consider the torque balance on sphere 1 in the inertialess limit, where the angular velocity of sphere 1 is modified by the hydrodynamic velocity $\mathbf{u}_2(\mathbf{x})$ induced by the motion of sphere 2 [47],

$$\mathbf{T}_1^e - 8\pi\eta a^3\big[\mathbf{\Omega}_1 - \tfrac{1}{2}\nabla\times\mathbf{u}_2(\mathbf{x}_1)\big] = 0. \qquad (38)$$

Here, $\mathbf{T}_1^e$ is the electric torque on sphere 1,

$$\mathbf{T}_1^e = -4\pi\varepsilon_1\mathbf{P}_1\times\nabla\phi_e^1(\mathbf{x}_1) + O(R^{-8}), \qquad (39)$$

where $\nabla\phi_e^1(\mathbf{x}_1)$ is given in Eq. (37), and where we have neglected the torque induced by the quadrupole moment [46]. To leading order, $\mathbf{u}_2(\mathbf{x})$ is given by the rotlet flow driven by the rotation of sphere 2 with angular velocity $\mathbf{\Omega}_2$ [47],

$$\mathbf{u}_2(\mathbf{x}) = a^3\mathbf{\Omega}_2\times\frac{(\mathbf{x}-\mathbf{x}_2)}{|\mathbf{x}-\mathbf{x}_2|^3} + O(R^{-5}), \qquad (40)$$

with vorticity at the location of sphere 1 given by

$$\nabla\times\mathbf{u}_2(\mathbf{x}_1) = -\frac{a^3}{R^3}\mathbf{\Pi}\cdot\mathbf{\Omega}_2 + O(R^{-6}). \qquad (41)$$

The order of the error in Eqs. (40) and (41) can be understood as follows: the rotlet flow $\mathbf{u}_1$ generated by sphere 1, which scales like $O(R^{-2})$ at the center of sphere 2, induces a stresslet on sphere 2, whose magnitude scales with the gradient of $\mathbf{u}_1$ as $O(R^{-3})$ and adds a contribution to $\mathbf{u}_2$ in Eq. (40) that decays like $O(R^{-5})$. Substituting Eqs. (39) and (41) into the torque balance Eq. (38) yields

$$\mathbf{\Omega}_1 + \frac{a^3}{2R^3}\mathbf{\Pi}\cdot\mathbf{\Omega}_2 = -\frac{\varepsilon_1}{2\eta a^3}\mathbf{P}_1\times\nabla\phi_e^1(\mathbf{x}_1) + O(R^{-6}), \quad (42)$$

and a similar equation can be written for the torque balance on sphere 2. These two coupled linear equations for $\mathbf{\Omega}_1$ and $\mathbf{\Omega}_2$

are easily solved analytically to leading order as

$$\mathbf{\Omega}_1 = \frac{\varepsilon_1}{2\eta a^3}\bigg\{\mathbf{P}_1\times\bigg(\mathbf{E}_0 - \frac{1}{R^3}\mathbf{\Pi}\cdot\mathbf{P}_2\bigg) \\ - \frac{a^3}{2R^3}\mathbf{\Pi}\cdot\bigg[\mathbf{P}_2\times\bigg(\mathbf{E}_0 - \frac{1}{R^3}\mathbf{\Pi}\cdot\mathbf{P}_1\bigg)\bigg]\bigg\}, \quad (43)$$

$$\mathbf{\Omega}_2 = \frac{\varepsilon_1}{2\eta a^3}\bigg\{\mathbf{P}_2\times\bigg(\mathbf{E}_0 - \frac{1}{R^3}\mathbf{\Pi}\cdot\mathbf{P}_1\bigg) \\ - \frac{a^3}{2R^3}\mathbf{\Pi}\cdot\bigg[\mathbf{P}_1\times\bigg(\mathbf{E}_0 - \frac{1}{R^3}\mathbf{\Pi}\cdot\mathbf{P}_2\bigg)\bigg]\bigg\}, \quad (44)$$

where the error in both equations is of order $O(R^{-6})$. Note that the last term in Eqs. (43) and (44) is itself of order $O(R^{-6})$; we retain it nonetheless as it is required for $\mathbf{\Omega}_1 = \mathbf{\Omega}_2 = \mathbf{0}$ to be an exact steady solution of the equations derived here.

3. Force balance

In the case of two freely suspended particles, translational motion is also expected to occur as a result of dielectrophoretic forces on the particles. Such forces were previously analyzed in detail using the method of reflections [42,46,48], and can be expressed as

$$\mathbf{F}_1 = -4\pi\varepsilon_1\bigg[\mathbf{P}_1\cdot\nabla\nabla\phi_e^1(\mathbf{x}_1) + \frac{1}{6}\mathbf{Q}_1:\nabla\nabla\nabla\phi_e^1(\mathbf{x}_1) + \cdots\bigg], \qquad (45)$$

with a similar expression for $\mathbf{F}_2$. To leading order, this expression simplifies to

$$\mathbf{F}_1 = -\frac{12\pi\varepsilon_1}{R^4}[(\mathbf{P}_1\cdot\widehat{\mathbf{R}})\mathbf{P}_2 + (\mathbf{P}_2\cdot\widehat{\mathbf{R}})\mathbf{P}_1 + (\mathbf{P}_1\cdot\mathbf{P}_2)\widehat{\mathbf{R}} \\ - 5(\mathbf{P}_1\cdot\widehat{\mathbf{R}})(\mathbf{P}_2\cdot\widehat{\mathbf{R}})\widehat{\mathbf{R}}] + O(R^{-9}), \qquad (46)$$

and by symmetry $\mathbf{F}_2 = -\mathbf{F}_1$. This dielectrophoretic force then enters the force balance on the sphere. Neglecting inertia, the force balance on sphere 1 is written

$$6\pi\eta a\bigg[\mathbf{U}_1 - \mathbf{u}_2(\mathbf{x}_1) - \frac{a^2}{6}\nabla^2\mathbf{u}_2(\mathbf{x}_1)\bigg] = \mathbf{F}_1, \qquad (47)$$

where the translational velocity $\mathbf{U}_1$ of the sphere is also modified by the flow field $\mathbf{u}_2$ induced by sphere 2 according to Faxén's law [47]. Noting that $\nabla^2\mathbf{u}_2(\mathbf{x}_1) = O(R^{-7})$, this yields the following expression for the particle velocities:

$$\mathbf{U}_1 = -\frac{a^3}{R^2}\mathbf{\Omega}_2\times\widehat{\mathbf{R}} + \frac{\mathbf{F}_1}{6\pi\eta a} + O(R^{-5}), \qquad (48)$$

$$\mathbf{U}_2 = \frac{a^3}{R^2}\mathbf{\Omega}_1\times\widehat{\mathbf{R}} + \frac{\mathbf{F}_2}{6\pi\eta a} + O(R^{-5}). \qquad (49)$$

In these equations, the leading-order error arises due to the Stokeslet flows driven by forces $\mathbf{F}_1$ and $\mathbf{F}_2$, which modify the velocities to order $O(R^{-5})$ and could easily be included for higher accuracy. The translational motion arises from two different processes: first, the spheres are advected by the rotlet flows they generate, which can lead to orbiting motions as we will see in numerical simulations in Sec. IV B; second, dielectrophoretic forces cause relative motions that can be either attractive or repulsive depending on the orientation of the electric dipoles on the spheres.

4. Nondimensionalization and summary of the governing equations

In the remainder of the paper, we scale all variables using the particle radius a, Maxwell-Wagner relaxation time τ_{MW}, and applied electric field strength E_0 as characteristic scales for length, time, and electric field, respectively. Under these scalings, one dimensionless group appears in the equations, which is the electric Mason number Ma characterizing the ratio of viscous to polarization forces,

$$\mathrm{Ma} = \frac{2\eta}{\tau_{\mathrm{MW}}\varepsilon_1 E_0^2}. \qquad (50)$$

The Mason number is directly related to the ratio of the applied field strength to the critical electric field E_c^0 for the onset of Quincke rotation of a single particle in the absence of interactions as

$$\mathrm{Ma} = (\varepsilon_{21} - \sigma_{21})\left(\frac{E_c^0}{E_0}\right)^2. \qquad (51)$$

After nondimensionalization, the governing equations can be summarized as follows. The electric dipoles $\mathbf{P}_1$ and $\mathbf{P}_2$ satisfy the two coupled ordinary differential equations,

$$\frac{d\mathbf{P}_1}{dt} = \boldsymbol{\Omega}_1 \times \left[\mathbf{P}_1 + \varepsilon_{21}\left(-\widehat{\mathbf{z}} + \frac{1}{R^3}\boldsymbol{\Pi}\cdot\mathbf{P}_2\right) \right]$$
$$- \left[\mathbf{P}_1 + \sigma_{21}\left(-\widehat{\mathbf{z}} + \frac{1}{R^3}\boldsymbol{\Pi}\cdot\mathbf{P}_2\right) \right], \qquad (52)$$

$$\frac{d\mathbf{P}_2}{dt} = \boldsymbol{\Omega}_2 \times \left[\mathbf{P}_2 + \varepsilon_{21}\left(-\widehat{\mathbf{z}} + \frac{1}{R^3}\boldsymbol{\Pi}\cdot\mathbf{P}_1\right) \right]$$
$$- \left[\mathbf{P}_2 + \sigma_{21}\left(-\widehat{\mathbf{z}} + \frac{1}{R^3}\boldsymbol{\Pi}\cdot\mathbf{P}_1\right) \right]. \qquad (53)$$

The angular velocities $\boldsymbol{\Omega}_1$ and $\boldsymbol{\Omega}_2$ can also be expressed in terms of the dipole moments through the torque balance on each sphere as

$$\boldsymbol{\Omega}_1 = \frac{1}{\mathrm{Ma}}\left\{ \mathbf{P}_1 \times \left(\widehat{\mathbf{z}} - \frac{1}{R^3}\boldsymbol{\Pi}\cdot\mathbf{P}_2\right) \right.$$
$$\left. - \frac{1}{2R^3}\boldsymbol{\Pi}\cdot\left[\mathbf{P}_2 \times \left(\widehat{\mathbf{z}} - \frac{1}{R^3}\boldsymbol{\Pi}\cdot\mathbf{P}_1\right)\right] \right\}, \qquad (54)$$

$$\boldsymbol{\Omega}_2 = \frac{1}{\mathrm{Ma}}\left\{ \mathbf{P}_2 \times \left(\widehat{\mathbf{z}} - \frac{1}{R^3}\boldsymbol{\Pi}\cdot\mathbf{P}_1\right) \right.$$
$$\left. - \frac{1}{2R^3}\boldsymbol{\Pi}\cdot\left[\mathbf{P}_1 \times \left(\widehat{\mathbf{z}} - \frac{1}{R^3}\boldsymbol{\Pi}\cdot\mathbf{P}_2\right)\right] \right\}. \qquad (55)$$

Finally, if the spheres are freely suspended, their translational velocities are given by

$$\mathbf{U}_1 = -\frac{1}{R^2}\boldsymbol{\Omega}_2 \times \widehat{\mathbf{R}} - \frac{4}{\mathrm{Ma}\,R^4}[(\mathbf{P}_1\cdot\widehat{\mathbf{R}})\mathbf{P}_2 + (\mathbf{P}_2\cdot\widehat{\mathbf{R}})\mathbf{P}_1$$
$$+ (\mathbf{P}_1\cdot\mathbf{P}_2)\widehat{\mathbf{R}} - 5(\mathbf{P}_1\cdot\widehat{\mathbf{R}})(\mathbf{P}_2\cdot\widehat{\mathbf{R}})\widehat{\mathbf{R}}], \qquad (56)$$

$$\mathbf{U}_2 = \frac{1}{R^2}\boldsymbol{\Omega}_1 \times \widehat{\mathbf{R}} + \frac{4}{\mathrm{Ma}\,R^4}[(\mathbf{P}_1\cdot\widehat{\mathbf{R}})\mathbf{P}_2 + (\mathbf{P}_2\cdot\widehat{\mathbf{R}})\mathbf{P}_1$$
$$+ (\mathbf{P}_1\cdot\mathbf{P}_2)\widehat{\mathbf{R}} - 5(\mathbf{P}_1\cdot\widehat{\mathbf{R}})(\mathbf{P}_2\cdot\widehat{\mathbf{R}})\widehat{\mathbf{R}}]. \qquad (57)$$

Equations (52) and (53) form a system of coupled nonlinear ordinary differential equations for the dipole moments, that are also coupled to Eqs. (54)–(57) for the angular and translational

motions of the spheres. This system of equations can analyzed theoretically as we do next in Sec. III, or integrated numerically as will be discussed in Sec. IV.

III. LINEAR STABILITY ANALYSIS

We first analyze the effects of electrohydrodynamic interactions on the onset of Quincke rotation by performing a linear stability analysis on the equations of Sec. II B 4 in the case where the two spheres are held fixed in space, so that the separation vector $\mathbf{R}$ does not change in time and the spheres only undergo rotational motion. In this case, the system of equations reduces to Eqs. (52)–(55). A steady base state exists in the absence of rotation: $\boldsymbol{\Omega}_1 = \boldsymbol{\Omega}_2 = \mathbf{0}$, in which case both dipole moments assume the same steady value $\mathbf{P}_0$ obtained by solution of Eqs. (52) and (53),

$$\mathbf{P}_1 = \mathbf{P}_2 = \mathbf{P}_0 = \frac{\sigma_{21}}{1 + \frac{\sigma_{21}}{R^3}}\left(\mathbf{I} + \frac{3\sigma_{21}}{R^3 - 2\sigma_{21}}\widehat{\mathbf{R}}\widehat{\mathbf{R}} \right)\cdot\widehat{\mathbf{z}}. \qquad (58)$$

In this equation, we see that electric interactions modify the steady dipole with a correction scaling as $O(R^{-3})$ that can have a nonzero component perpendicular to the field depending on the orientation of the spheres. Next, we perturb the steady-state dipole by a small amount

$$\mathbf{P}_1(t) = \mathbf{P}_0 + \epsilon\mathbf{p}_1(t), \quad \mathbf{P}_2(t) = \mathbf{P}_0 + \epsilon\mathbf{p}_2(t), \qquad (59)$$

which induces weak rotations

$$\boldsymbol{\Omega}_1(t) = \epsilon\boldsymbol{\omega}_1(t), \quad \boldsymbol{\Omega}_2(t) = \epsilon\boldsymbol{\omega}_2(t). \qquad (60)$$

Linearization of the governing equations easily yields a homogeneous system of coupled linear ordinary differential equations for the perturbation dipoles

$$\frac{d\mathbf{p}_1}{dt} = \left(1 - \frac{\varepsilon_{21}}{\sigma_{21}}\right)\boldsymbol{\omega}_1 \times \mathbf{P}_0 - \mathbf{p}_1 - \frac{\sigma_{21}}{R^3}\boldsymbol{\Pi}\cdot\mathbf{p}_2, \qquad (61)$$

with a similar equation for $\mathbf{p}_2(t)$. In Eq. (61), the linearized angular velocity $\boldsymbol{\omega}_1$ is expressed as

$$\boldsymbol{\omega}_1 = \frac{1}{\mathrm{Ma}}\left\{ \frac{1}{\sigma_{21}}\mathbf{p}_1 \times \mathbf{P}_0 - \frac{1}{R^3}\mathbf{P}_0 \times (\boldsymbol{\Pi}\cdot\mathbf{p}_2) \right.$$
$$\left. - \frac{1}{2R^3}\boldsymbol{\Pi}\cdot\left[\frac{1}{\sigma_{21}}\mathbf{p}_2 \times \mathbf{P}_0 - \frac{1}{R^3}\mathbf{P}_0 \times (\boldsymbol{\Pi}\cdot\mathbf{p}_1) \right] \right\}. \qquad (62)$$

with a similar expression for $\boldsymbol{\omega}_2$. Equations (61) and (62), together with equivalent expressions for $\mathbf{p}_2$ and $\boldsymbol{\omega}_2$, can be written in the form

$$\frac{d}{dt}\begin{bmatrix} \mathbf{p}_1 \\ \mathbf{p}_2 \end{bmatrix} = \mathbf{J}(\mathrm{Ma}, \varepsilon_{21}, \sigma_{21}, \mathbf{R})\cdot\begin{bmatrix} \mathbf{p}_1 \\ \mathbf{p}_2 \end{bmatrix}, \qquad (63)$$

where the 6×6 Jacobian matrix $\mathbf{J}$ is a function of the Mason number Ma (or equivalently of E_0/E_c^0), of the dimensionless material parameters ε_{21} and σ_{21}, and of the dimensionless separation vector $\mathbf{R}$ between the two spheres. Note that while the matrix $\mathbf{J}$ depends on the separation vector $\mathbf{R}$, its eigenvalues really only depend on the dimensionless distance R between the sphere centers and on the angle $\Theta = \cos^{-1}(\widehat{\mathbf{R}}\cdot\widehat{\mathbf{z}})$ defining the orientation of the sphere pair with respect to the external field direction. The explicit form of $\mathbf{J}$, which is quite cumbersome, is omitted here for brevity.
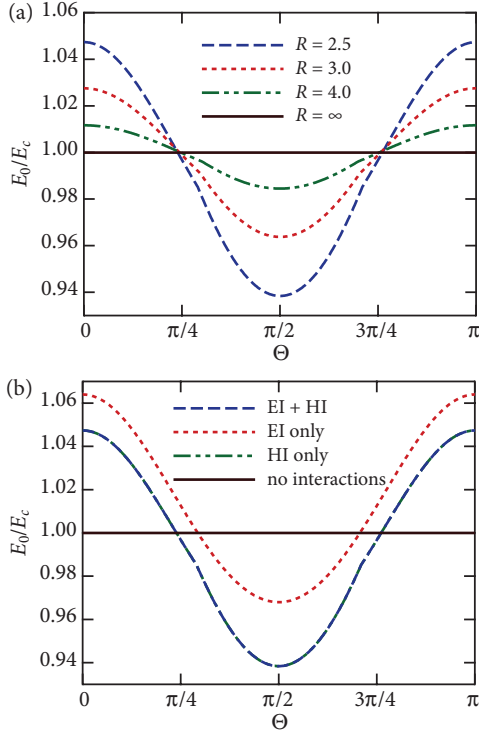
FIG. 5. (Color online) Results of the linear stability analysis. (a) Critical electric field E_c in the presence of interactions (normalized by the critical field E_c^0 for onset of Quincke rotation of an isolated particle) as a function of the orientation angle Θ between the pair of spheres and the field direction, for various values of the separation distance R. (b) Critical electric field E_c/E_c^0 as a function of Θ for $R = 2.5$, when either electric interactions (EIs), hydrodynamic interactions (HIs), or both are taken into account. In (b), note that the two curves for EI + HI and for HI only fall exactly on top of each other. In this figure, the materials parameters ε_{21} and σ_{21} were chosen as in the recent experiments of Lemaire and coworkers [29–32] to be $\varepsilon_{21} = -0.1097$ and $\sigma_{21} = -0.5$.

The eigenvalues λ of the Jacobian **J**, which can be calculated numerically, determine the stability of the base state with no rotation. Their real parts are the actual growth rates, and a positive growth rate indicates the exponential growth of any small perturbation of the base-state dipole moment of Eq. (58), subsequently leading to Quincke rotation of the particles. A numerical solution of the eigenvalue problem shows that the Jacobian has six real eigenvalues, which are all negative when there is no electric field. As the field strength is increased, some of them become positive indicating the onset of Quincke rotation. The critical field value E_c above which instability occurs is plotted as a function of the orientation Θ of the spheres in Fig. 5(a), where it is normalized by the critical field E_c^0 obtained in Eq. (33) in the absence of interactions. The effect of interactions is subtle and can either increase or decrease the value of the critical electric field depending on Θ: for spheres that are nearly aligned with the field (Θ close to 0 or π), the critical electric field increases, corresponding to a stabilizing effect of interactions, whereas it decreases when the pair of spheres is aligned in a direction perpendicular to the applied field (Θ close to $\pi/2$), corresponding to a destabilizing effect. These effects are clearest when the particles are close to

one another, and as the distance R increases, the critical electric field asymptotically tends to the critical field E_c^0 for an isolated sphere. The dependence of E_c on R can also be probed and shows that $E_c/E_c^0 - 1 = O(R^{-3})$ for $R \gg 1$, as could have been anticipated from the form of the governing equations.

The respective roles of electric and hydrodynamic interactions on the stability can be further analyzed by solving two additional eigenvalue problems in which either type of interaction is turned off. The results for the critical field in these various cases are plotted in Fig. 5(b), for a fixed distance of $R = 2.5$. When only electric interactions are taken into account, the critical electric field shows a similar dependence on Θ as when both types of interactions are included, indicating a stabilizing effect of electric interactions for a pair of spheres aligned with the field but a destabilizing effect for spheres aligned perpendicular to the field; however, the critical value of the electric field is always larger than when hydrodynamic interactions are included, suggesting that hydrodynamic interactions play a more important role in the onset of rotation than electric interactions. This is indeed confirmed when electric interactions are turned off, in which case the critical electric field E_c is the same as for the full system of equations: this curious observation suggests that hydrodynamic modes are the ones that govern the modification of the onset of instability by interactions.

IV. NUMERICAL SIMULATIONS

While the linear stability analysis of Sec. III provided results on the onset of rotation in the presence of interactions, nonlinear dynamics can only be studied numerically. In this section, we present results from numerical simulations of the unsteady governing equations, which were integrated using a fourth-order Runge-Kutta time-marching scheme. We first consider the case of two spheres that are fixed in space but free to rotate in Sec. IV A, and then turn to the case of freely suspended spheres in Sec. IV B. In all simulations, the initial dipole moments are given by Eq. (58) but are weakly perturbed by infinitesimal random vectors with components of magnitude of the order of 10^{-3}. For both fixed and freely suspended spheres, we note a very strong sensitivity of the solution on the infinitesimal initial perturbation introduced in the system. Therefore, we focus the discussion on a few representative cases as well as on the statistics for the steady states obtained over many realizations with different random initial perturbations. In all of this section, the two dimensionless material constants ε_{21} and σ_{21} are set to $\varepsilon_{21} = -0.1097$ and $\sigma_{21} = -0.5$, which correspond to the experiments of Lemaire and coworkers [29–32] and were also the values used by Huang *et al.* [34].

A. Fixed spheres

A typical simulation in the case of two fixed spheres in a field of magnitude $E_0 = 1.5 E_c^0$ is shown in Fig. 6, where both the components and magnitude of the angular velocities are plotted as functions of time. The infinitesimal perturbation introduced to the system at $t = 0$ is found to amplify with time and lead to the growth of the angular velocities, which briefly oscillate and reach steady values. The steady-state angular velocities are always found to have zero components in the
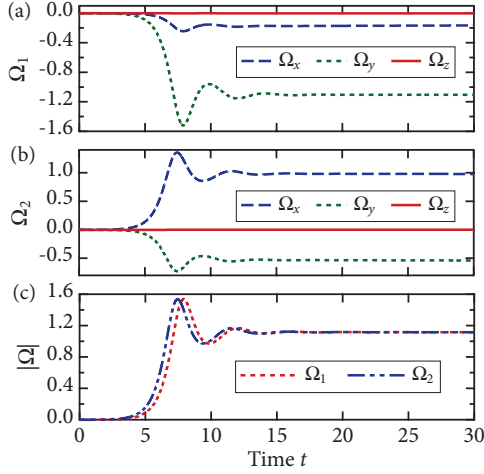
FIG. 6. (Color online) Angular velocities in a simulation of two fixed interacting spheres separated by a distance $R = 10$ undergoing Quincke rotation in an applied electric field of magnitude $E_0 = 1.5\,E_c^0$: (a) angular velocity $\boldsymbol{\Omega}_1$ of the first sphere as a function of time; (b) angular velocity $\boldsymbol{\Omega}_2$ of the second sphere; (c) angular velocity magnitudes.

field direction as in the single-sphere case. Quite interestingly, the magnitudes Ω_1 and Ω_2 of the angular velocities are found to converge to the same value, even though the directions of rotation are not the same. This peculiar result, which we cannot explain theoretically, is observed systematically in all simulations. The final direction of rotation in the x-y plane depends sensitively on the initial perturbation, but the steady magnitude of the angular velocity varies only weakly between simulations at fixed values of R, Θ, and E_0. The effect of further increasing the electric field is shown in Fig. 7, where Ω_1 and Ω_2 are plotted vs time for two simulations with $E_0/E_c^0 = 3.0$ and 6.0. We find that stronger fields result in stronger and faster oscillations during the initial transient, but these oscillations always subside and give way to synchronization of the angular velocity magnitudes.

Next, we analyze statistics of the steady angular velocity reached after the initial transient oscillations. We report averages over larger numbers ($\geqslant 200$) of simulations with different
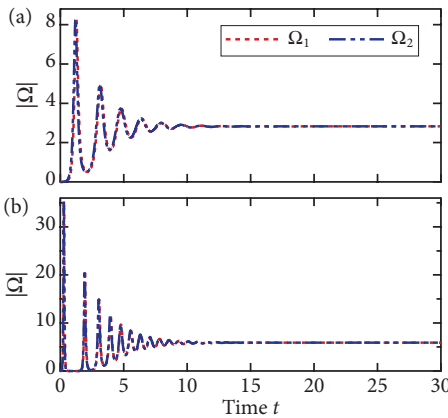

FIG. 7. (Color online) Angular velocities as functions of time in two simulations with $R = 10$ at different field strengths: (a) $E_0/E_c^0 = 3.0$, (b) $E_0/E_c^0 = 6.0$.
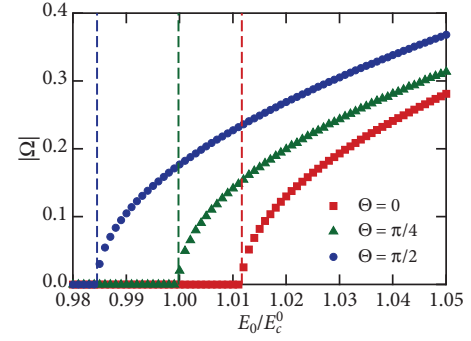

FIG. 8. (Color online) Onset of Quincke rotation of two interacting spheres: the plot shows the average steady-state angular velocity as a function of the applied electric field E_0 for two spheres separated by a distance $R = 4.0$ and for various orientations Θ. The vertical dashed lines show the critical electric field strengths E_c/E_c^0 for onset of rotation predicted by the linear stability analysis of Sec. III.

small random initial perturbations. Throughout this section, we also compare these statistics to an asymptotic estimate of the steady-state angular velocity derived in Appendix A in the case of corotating spheres in the limit of $R \gg 1$

$$\langle \Omega^2 \rangle = \Omega_0^2 + \frac{1 + 3 \cos 2\Theta}{R^3} \left[\varepsilon_{21} \left(\frac{E_0}{E_c^0} \right)^2 + (\sigma_{21} - \varepsilon_{21}) \right],$$

(64)

where $\Omega_0^2 = (E_0/E_c^0)^2 - 1$ denotes to the steady-state angular velocity of an isolated sphere.
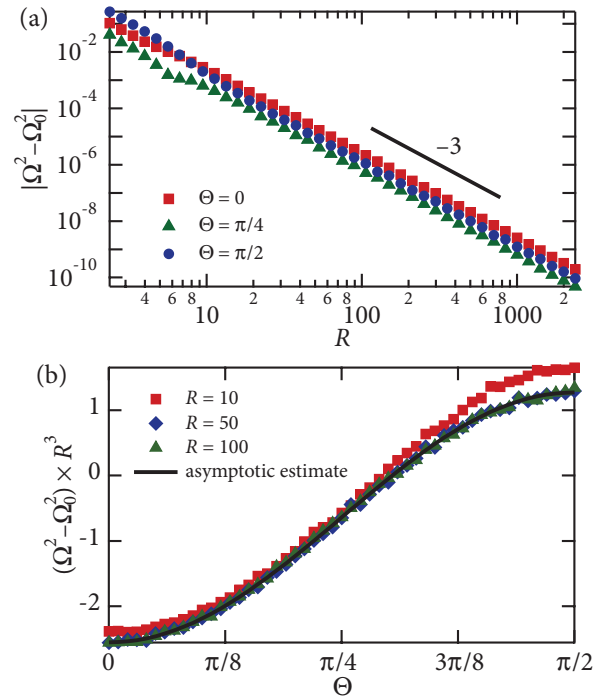

FIG. 9. (Color online) Dependence of the deviation $(\Omega^2 - \Omega_0^2)$ of the steady-state angular velocity from the isolated sphere value on: (a) the distance R between the spheres, and (b) the orientation Θ of the sphere pair with respect to the field direction. Both plots were obtained for $E_0/E_c^0 = 1.5$. In (b), the simulation results are compared to the asymptotic result of Eq. (64).
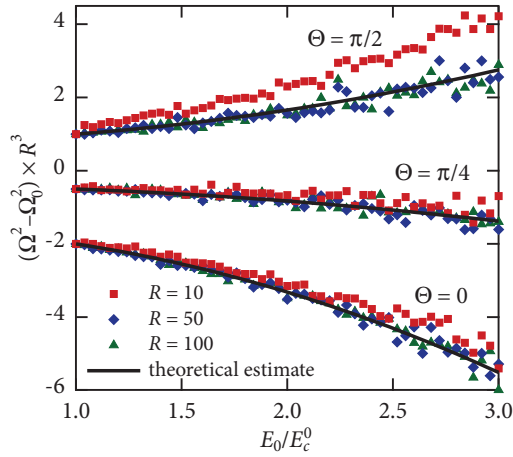
FIG. 10. (Color online) Dependence of $(\Omega^2 - \Omega_0^2) \times R^3$ on electric field strength E_0 above the onset of Quincke rotation, for different values of Θ and R. The simulation results are compared to the asymptotic prediction of Eq. (64).

The onset of Quincke rotation in the case of two interacting spheres is illustrated in Fig. 8, where the steady-state angular velocity magnitude is plotted as a function of the applied field and is seen to undergo a pitchfork bifurcation at a critical electric field. In excellent agreement with the results of the linear stability analysis of Sec. III, the value of the critical electric field depends on the orientation Θ of the spheres, with $\Theta = 0$ as the most stable orientation and $\Theta = \pi/2$ as the

most unstable one. As the distance R between the two spheres increases, the value of Ω converges towards the single-sphere solution Ω_0 with a bifurcation at $E_0 = E_c^0$.

The precise dependence of the steady-state angular velocity on R and Θ is shown in Fig. 9. The deviation $\Omega^2 - \Omega_0^2$ between the angular velocity in the presence of interactions and that of an isolated sphere is plotted in Fig. 9(a) and is observed to decay rapidly as $1/R^3$, as could have easily been anticipated from the form of the governing equations and in agreement with the asymptotic estimate of Eq. (64). The sign of this deviation depends again on the orientation of the spheres: interactions tend to decrease the rate of rotation for spheres aligned with the field direction and increase it for spheres aligned in a perpendicular direction. The functional dependence on Θ is plotted in Fig. 9(b) and agrees quite well with Eq. (64) as soon as $R \gtrsim 10$.

Figure 10 shows the effect of field strength E_0 on the angular velocity above the bifurcation. Increasing field strength increases the effect of interactions with a quadratic dependence on E_0/E_c^0, and all the results for different values of Θ and R are found to collapse remarkably well onto the asymptotic approximation of Eq. (64), which provides an excellent prediction for the angular velocity regardless of the directions of rotation when R is sufficiently large.

B. Freely suspended spheres

We now turn our attention to the dynamics of freely suspended spheres, whose relative motion results from the
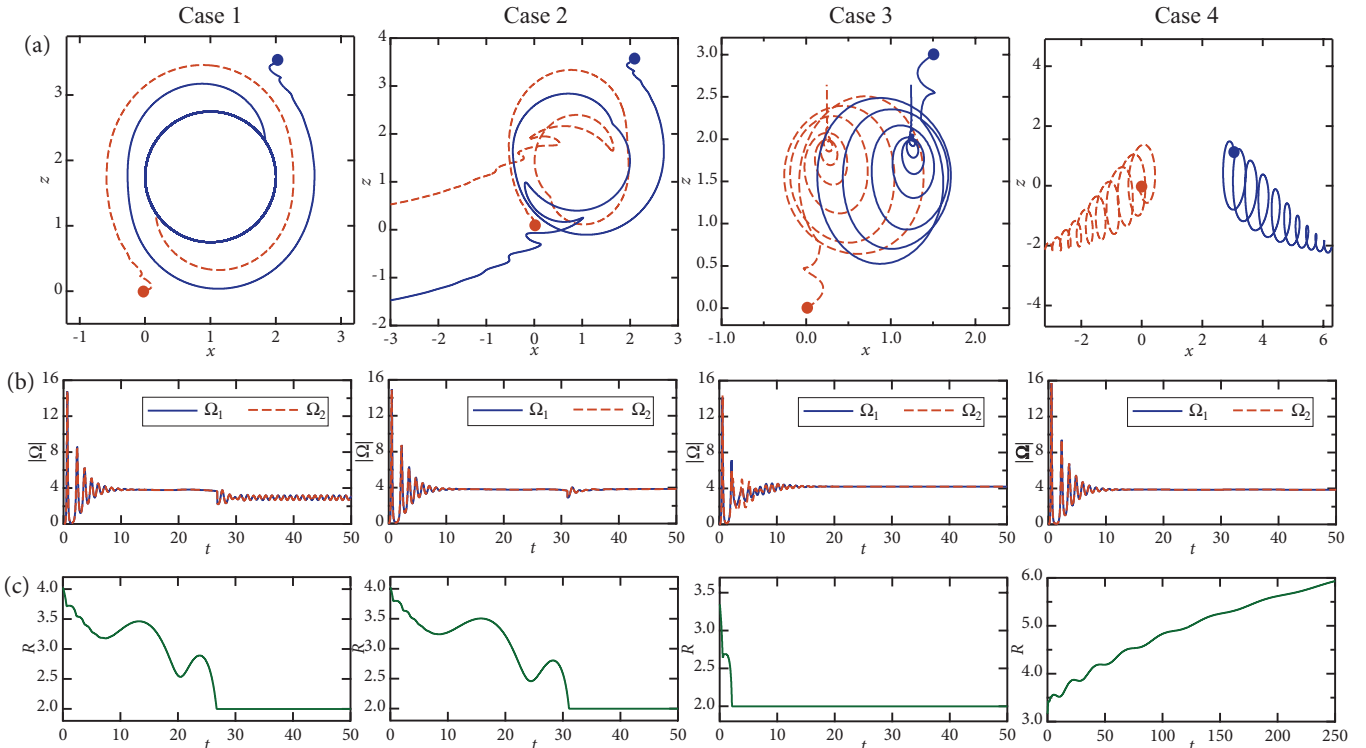

FIG. 11. (Color online) Dynamics of freely suspended spheres: (a) typical particle trajectories (where the two dots mark the initial position of the particles), (b) magnitude of the angular velocities vs time, and (c) separation distance vs time. Depending on the relative position of the spheres and on the infinitesimal initial perturbation introduced in the system, four different types of motions are observed, as illustrated in cases 1–4. In this plot, $E_0/E_c^0 = 4.0$, $\varepsilon_{21} = -0.1097$ and $\sigma_{21} = -0.5$. Also see the accompanying online movie [49].

combination of the rotlet flows generated by the sphere rotations and of the dielectrophoretic forces (dipole-dipole interactions) as discussed in Sec. II B 3. As we show below, dielectrophoretic forces can result in the pairing of the particles, in which case we implement a contact algorithm to prevent particle overlap. The algorithm assumes rolling without slipping between the two sphere surfaces and is explained in more detail in Appendix B. It is important to note that the calculation of electrohydrodynamic interactions used here is based on the assumption of widely separated spheres, and is therefore likely inaccurate when the two particles are near contact. This should be borne in mind when analyzing the simulations presented here, and it is difficult to anticipate how the observed dynamics would change in the near field if a more accurate calculation of interactions were used (for instance based on a boundary integral formulation).

As in the case of fixed spheres, we observe a strong sensitivity of the dynamics to the initial perturbation introduced in the system at $t = 0$. Using numerical experiments, we

have identified four different types of qualitatively different behaviors, which are illustrated in Fig. 11 and accompanying online movie [49]. Case 1 corresponds to the somewhat artificial situation where no perturbation is introduced in the system. In this case, the motion of the two spheres as a result of dielectrophoresis is sufficient to destabilize the system and induce rotation. The dynamics of the sphere pair is perfectly two dimensional, and the particles are observed to undergo a spiraling motion during which their separation distance decreases leading to pairing up. The spiraling motion, which is observed in many trajectories (including in cases 2 and 3), is a consequence of the rotlet flows generated by the spinning spheres. Upon pairing, the spheres in case 1 continue to orbit around one another ad infinitum. In a physical system, small perturbations are expected to occur leading to cases 2, 3, and 4. In cases 2 and 3, the particles are also observed to pair up, though their motion is three dimensional. In case 2, pairing up eventually leads to alignment of the two spheres in the direction of the applied field and counterrotation in a normal direction, which causes them to translate as a pair in a horizontal direction at a constant velocity once steady state has been reached. In case 3, which is found to occur most rarely, pairing of the spheres leads to orbiting motions that eventually stabilize to a steady configuration in which the
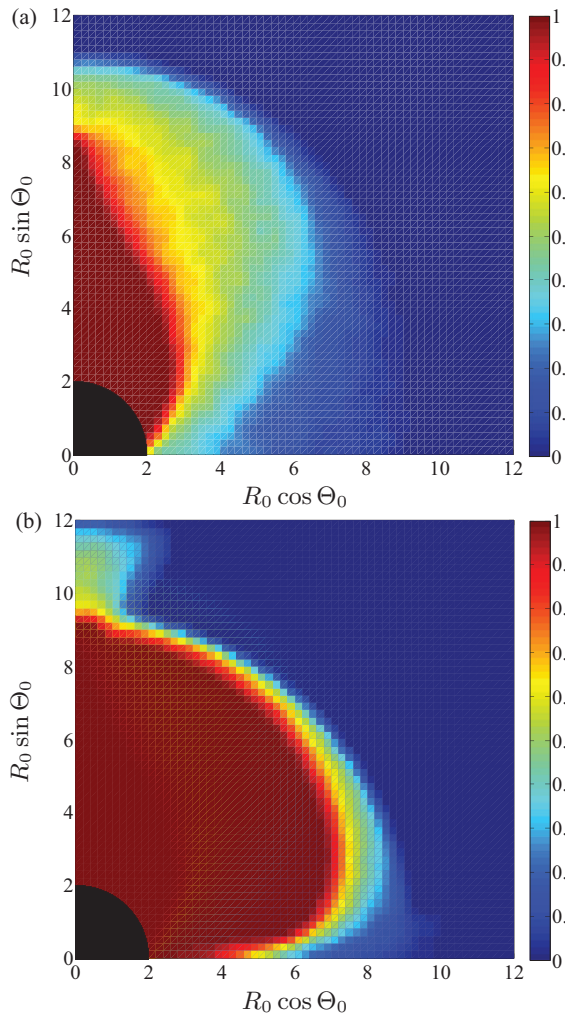

FIG. 12. (Color online) Probability of the two spheres pairing up (cases 1, 2, and 3) vs separating (case 4) as a function of $R_0 = |\mathbf{R}_0|$ and $\Theta_0 = \cos^{-1}(\mathbf{R}_0 \cdot \hat{\mathbf{z}}/R_0)$, where $\mathbf{R}_0 = \mathbf{R}(t = 0)$ is the initial separation vector between the spheres: (a) $E_0/E_c^0 = 4.0$, and (b) $E_0/E_c^0 = 6.0$. The black quarter disk centered at the origin corresponds to the region of excluded volume.
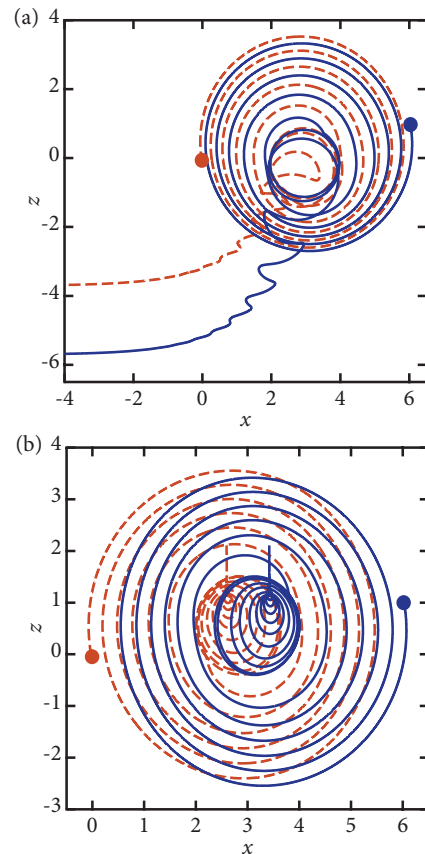

FIG. 13. (Color online) Typical particle trajectories for $E_0/E_c^0 = 6.0$, $\varepsilon_{21} = -0.1097$ and $\sigma_{21} = -0.5$: plots (a) and (b) show two different types of trajectories corresponding, respectively, to cases 2 and 3 of Fig. 11. In this plot, the two dots mark the initial positions of the particles.

spheres are aligned in a direction perpendicular to the electric field and corotate around their axis of centers while remaining stationary in space. Finally, in case 4 the two spheres do not pair up but rather slowly separate in space as a result of dipolar interactions while steadily rotating.

The outcome of a particular simulation is difficult to predict based solely on the initial configuration of the spheres, as different infinitesimal perturbations can lead to any of cases 2 to 4. To quantify this subtle dependence, we show in Fig. 12(a) the probability of pairing (cases 1, 2, and 3) vs separation (case 4) as a function of the initial distance R_0 between the spheres and of their initial orientation Θ_0 with respect to the field direction, for the same electric field strength as in Fig. 11 ($E_0/E_c^0 = 0.4$). We observe that initial configurations in which the spheres are initially nearly aligned with the electric field are more likely to lead to particle pairing, which could have been anticipated based on the form of the dielectrophoretic forces which are attractive for such configurations [13,42,50]. However, many initial values of R_0 and Θ_0 are seen to equally lead to either pairing or separation. The effect of increasing field strength is shown in Fig. 12(b), where the pairing probability is plotted for $E_0/E_c^0 = 6.0$. In this stronger field, we find that the region of high pairing probability extends further away from the field axis, indicating a stronger likelihood of pairing events at high values of E_0. Typical trajectories for the value of $E_0/E_c^0 = 6.0$ are shown in Fig. 13. These trajectories, which correspond to cases 2 and 3, show similar characteristics as in Fig. 11 but exhibit stronger orbiting motions, which we find to be a feature of all simulations in strong fields.

V. CONCLUDING REMARKS

In summary, we have developed an analytical model for the Quincke rotation of a pair of identical spherical particles that are interacting both electrically and hydrodynamically. The modeling of Quincke rotation is based on the classic Taylor-Melcher leaky dielectric model and on an asymptotic description of interactions using the method of reflections, which is valid for widely separated particles. We have only retained leading-order electric and hydrodynamic effects, which result from electric dipole-dipole interactions and from hydrodynamic rotlet interactions due to the spinning of the spheres, respectively, and we note that both types of interactions modify the dipoles and angular velocities of the spheres to order $O(R^{-3})$. Using a linear stability analysis in the case where the two spheres are fixed in space, we have shown that interactions can either have a stabilizing or destabilizing effect on the onset for rotation depending on the orientation of the sphere pair with respect to the field direction, and that the leading effect of interactions on this onset is of hydrodynamic origin.

Numerical simulations of the governing equations have also been performed for both fixed spheres and freely suspended spheres. In all of these simulations, we always observed synchronization of the angular velocity magnitudes, though the axes of rotation of the two spheres are not the same in general. In the case of spheres that are held fixed in space, Quincke rotation of the spheres only occurs above a critical electric field that matches the prediction of the stability analysis, and

the time dynamics in the unstable regime are characterized by transient oscillations leading to synchronization at a steady angular velocity. The steady-state angular velocity magnitude and direction depend sensitively upon the configuration of the spheres and initial perturbation to the system, though we find that the statistics of the mean angular velocity magnitude $\langle \Omega^2 \rangle$ are well described by a theoretical estimate derived for corotating spheres.

In the case of freely suspended spheres, relative motion of the particles also occurs as a result of the hydrodynamic flow driven by particle rotations and of the dielectrophoretic forces on the particles due to multipolar electric interactions. Numerical experiments have shown that these interactions can lead to complex particle trajectories, which we categorized into four cases: (i) two-dimensional spiraling motion leading to pairing and spinning of the particle pair about the point of contact (only observed in the absence of any initial perturbation), (ii) spiraling motion leading to pairing in the field direction with counterrotation of the spheres and translation as a pair in a direction perpendicular to the field, (iii) spiraling motion leading to pairing and alignment in a direction perpendicular to the field with corotation of the spheres about their axis of center, and (iv) slow separation of the spheres accompanied with spiraling trajectories. The outcome of a particular simulation depends on both the orientation of the spheres and the initial perturbation to the system. Increasing field strength is observed to increase the probability of trajectories leading to pairing, as well as cause more pronounced spiraling motions. It should be kept in mind, however, that the model solved is accurate for widely separated particles and that near-field interactions may lead to different dynamics in a physical experiment, in particular in cases where pairing occurs. A more accurate treatment of near-contact motions would require a different numerical model, for instance based on the boundary element method.

One important conclusion of this work is the important role of hydrodynamic interactions, which had been neglected in previous studies [40,41]. In fact, our asymptotic model demonstrated that, perhaps surprisingly, hydrodynamic interactions modify the dipole relaxation equations at the same asymptotic order as electric dipole-dipole interactions. It was also noted that the onset of instability for two interacting spheres is primarily affected by hydrodynamic interactions, and that the spatial dynamics in simulations of freely suspended spheres show a strong influence of rotlet interactions which cause orbiting and spiraling motions.

The present study has cast new light on the effects of electrohydrodynamic interactions on Quincke rotation in the simplest case of two identical spherical particles, and demonstrated a wide variety of dynamical behaviors resulting from the strongly nonlinear nature of the system. The effects of such complex pair interactions in large-scale suspensions of many interacting particles remain, however, difficult to anticipate, and may include structure formation on multiple scales and complex chaotic or correlated motions. We also expect these dynamics and patterns to be modified by an external flow, a situation of interest for the modeling of rheological experiments [29–33]. Some of these effects will be addressed in future work using numerical simulations by extending efficient algorithms previously developed by Park

and Saintillan [13,50] for nonlinear electrokinetic interactions in colloidal suspensions.

APPENDIX A: ASYMPTOTIC ESTIMATE OF THE STEADY-STATE ANGULAR VELOCITY

In this Appendix, we derive an asymptotic expression for the steady-state angular velocity of two interacting spheres that are fixed in space, in the case where the spheres are corotating: $\mathbf{\Omega}_1 = \mathbf{\Omega}_2 = \mathbf{\Omega}$. In this case, it is also obvious by symmetry that $\mathbf{P}_1 = \mathbf{P}_2 = \mathbf{P}$. We seek an expression for the correction to the steady-state angular velocity $\Omega_0 = |\mathbf{\Omega}_0|$ and dipole moment $\mathbf{P}_0$ of an isolated sphere to account for leading-order interactions in the limit of large separation distance $R \gg 1$. The single-sphere case was solved in Sec. II A, where we obtained in dimensionless variables

$$\mathbf{P}_0 = -A_1^0 \mathbf{\Omega}_0 \times \widehat{\mathbf{z}} + A_2^0 \widehat{\mathbf{z}}, \quad \Omega_0^2 = \left(\frac{E_0}{E_c^0}\right)^2 - 1, \quad \text{(A1)}$$

with

$$A_1^0 = \frac{\varepsilon_{21} - \sigma_{21}}{1 + \Omega_0^2}, \quad A_2^0 = \varepsilon_{21} - A_1^0. \quad \text{(A2)}$$

When interactions are taken into account, the dipole relaxation equation (52) at steady state simplifies to

$$\mathbf{\Omega} \times (\mathbf{P} + \varepsilon_{21}\mathbf{E}_e) - (\mathbf{P} + \sigma_{21}\mathbf{E}_e) = \mathbf{0}, \quad \text{(A3)}$$

where $\mathbf{E}_e = -\widehat{\mathbf{z}} + \mathbf{\Pi} \cdot \mathbf{P}/R^3$ is the electric field experienced by each sphere. To leading order, this can be approximated as $\mathbf{E}_e \approx -\widehat{\mathbf{z}} + \mathbf{\Pi} \cdot \mathbf{P}_0/R^3$, where $\mathbf{P}_0$ is given in Eq. (A1). The dipole moment equation (A3) can then be inverted for $\mathbf{P}$ as

$$\mathbf{P} = A_1 [\mathbf{\Omega} \times \mathbf{E}_e + (\mathbf{\Omega} \cdot \mathbf{E}_e)\mathbf{\Omega}] - A_2\mathbf{E}_e, \quad \text{(A4)}$$

where A_1 and A_2 are defined as in Eq. (A2) but with Ω_0 replaced by Ω. This expression can then be substituted into the torque balance equation (54), which becomes

$$\mathbf{\Omega} = \frac{A_1}{\text{Ma}} \Bigg[E_e^2 \mathbf{\Omega} - (\mathbf{\Omega} \cdot \mathbf{E}_e)\mathbf{E}_e - (\mathbf{\Omega} \cdot \mathbf{E}_e)(\mathbf{\Omega} \times \mathbf{E}_e) + \frac{1}{R^3}(\mathbf{I} - \widehat{\mathbf{z}}\widehat{\mathbf{z}}) \cdot \mathbf{\Omega}_0 \Bigg], \quad \text{(A5)}$$

where we have only kept leading-order corrections in $1/R^3$. Equation (A5) is a nonlinear equation for the angular velocity $\mathbf{\Omega}$; as in the single-sphere case, it does not admit a unique solution as the direction of rotation is indeterminate. However, it can be used to obtain an expression for the magnitude of the angular velocity. To this end, we assume an asymptotic expansion for $\mathbf{\Omega}$ of the form

$$\mathbf{\Omega} = \mathbf{\Omega}_0 + \frac{\boldsymbol{\alpha}}{R} + \frac{\boldsymbol{\beta}}{R^2} + \frac{\boldsymbol{\gamma}}{R^3} + O(R^{-4}), \quad \text{(A6)}$$

where $\boldsymbol{\alpha}$, $\boldsymbol{\beta}$, and $\boldsymbol{\gamma}$ are unknown vectors. The corresponding expansion for the magnitude of the angular velocity is also

given by

$$\Omega^2 = \Omega_0^2 + \frac{1}{R}(2\mathbf{\Omega}_0 \cdot \boldsymbol{\alpha}) + \frac{1}{R^2}(2\mathbf{\Omega}_0 \cdot \boldsymbol{\beta} + \alpha^2) + \frac{2}{R^3}(\mathbf{\Omega}_0 \cdot \boldsymbol{\gamma} + \boldsymbol{\alpha} \cdot \boldsymbol{\beta}) + O(R^{-4}). \quad \text{(A7)}$$

By substituting these expansions into Eq. (A5), where care must be taken to also expand A_1 which is also a function of Ω, one can derive a hierarchical set of conditions on the unknown vectors $\boldsymbol{\alpha}$, $\boldsymbol{\beta}$, and $\boldsymbol{\gamma}$ by successively identifying terms corresponding to various powers of $1/R$. At zeroth order, we recover the solution for an isolated particle, as expected. At first, second, and third orders, the conditions obtained are

$$\text{order } O(R^{-1}): \quad \boldsymbol{\alpha} \cdot \widehat{\mathbf{z}} = 0, \quad \mathbf{\Omega}_0 \cdot \boldsymbol{\alpha} = 0, \quad \text{(A8)}$$

$$O(R^{-2}): \quad \boldsymbol{\beta} \cdot \widehat{\mathbf{z}} = 0, \quad 2\mathbf{\Omega}_0 \cdot \boldsymbol{\beta} + \alpha^2 = 0, \quad \text{(A9)}$$

$$O(R^{-3}): \quad \mathbf{\Omega}_0 \cdot \boldsymbol{\gamma} + \boldsymbol{\alpha} \cdot \boldsymbol{\beta} = (1 + \Omega_0^2)\big[(\mathbf{\Pi} : \mathbf{\Omega}_0\mathbf{\Omega}_0)/4\Omega_0^2 - \widehat{\mathbf{z}} \cdot \mathbf{\Pi} \cdot \mathbf{P}_0\big]. \quad \text{(A10)}$$

While these conditions are not sufficient to solve for the vectors $\boldsymbol{\alpha}$, $\boldsymbol{\beta}$, and $\boldsymbol{\gamma}$, they are sufficient to fully obtain the unknown coefficients in the expansion of Ω^2 in Eq. (A7), which becomes

$$\Omega^2 = \Omega_0^2 + \frac{2}{R^3}(1 + \Omega_0^2)\left(\frac{\mathbf{\Pi} : \mathbf{\Omega}_0\mathbf{\Omega}_0}{4\Omega_0^2} - \widehat{\mathbf{z}} \cdot \mathbf{\Pi} \cdot \mathbf{P}_0\right) + O(R^{-4}). \quad \text{(A11)}$$

This expression shows that electric and hydrodynamic interactions modify the angular velocity of the spheres to order $O(R^{-3})$, though the perturbation depends on the direction of rotation through $\mathbf{\Omega}_0$ and on the orientation of the spheres through the tensor $\mathbf{\Pi}$. To obtain a more general estimate for the angular velocity that does not depend on the direction of rotation, we take an average of Eq. (A11) over all orientations of $\mathbf{\Omega}_0$, which after algebra yields the simple expression

$$\langle \Omega^2 \rangle = \Omega_0^2 + \frac{1 + 3\cos 2\Theta}{R^3}\left[\varepsilon_{21}\left(\frac{E_0}{E_c^0}\right)^2 + (\sigma_{21} - \varepsilon_{21})\right] + O(R^{-4}), \quad \text{(A12)}$$

in terms of the angle $\Theta = \cos^{-1}(\widehat{\mathbf{R}} \cdot \widehat{\mathbf{z}})$ between the field direction and the direction of the line of centers. While this expression was obtained for two corotating spheres, we show in Sec. IV that it provides a very good approximation to the steady-state angular velocity in the limit of $R \gg 1$ even when the two spheres are rotating in different directions.

We also note that Eq. (A12) can be used to provide an estimate for the critical field E_c in the presence of interactions by solving for the field value for which $\langle \Omega^2 \rangle = 0$,

$$E_c \approx E_c^0 \sqrt{\frac{(1 + 3\cos 2\Theta)(\varepsilon_{21} - \sigma_{21}) + R^3}{(1 + 3\cos 2\Theta)\varepsilon_{21} + R^3}}, \quad \text{(A13)}$$

which can be compared to the numerical results of the linear stability analysis of Sec. III and shows excellent agreement for $R \gg 1$.

APPENDIX B: CONTACT ALGORITHM

In the simulations of freely suspended spheres, particle overlap is prevented by introducing additional equal and opposite contact forces $\mathbf{F}^c = \mathbf{F}_1^c = -\mathbf{F}_2^c$ at the point of contact between the two touching particles. These forces modify both the torque and force balances on the spheres. The torque balance of Eq. (42) becomes, in dimensionless form,

$$\boldsymbol{\Omega}_1 + \frac{1}{2R^3}\boldsymbol{\Pi}\cdot\boldsymbol{\Omega}_2$$
$$= \frac{1}{\mathrm{Ma}}\left[\mathbf{P}_1 \times \left(\widehat{\mathbf{z}} - \frac{1}{R^3}\boldsymbol{\Pi}\cdot\mathbf{P}_2\right) + \frac{1}{4\pi}\widehat{\mathbf{R}}\times\mathbf{F}^c\right], \quad (B1)$$

$$\boldsymbol{\Omega}_2 + \frac{1}{2R^3}\boldsymbol{\Pi}\cdot\boldsymbol{\Omega}_1$$
$$= \frac{1}{\mathrm{Ma}}\left[\mathbf{P}_2 \times \left(\widehat{\mathbf{z}} - \frac{1}{R^3}\boldsymbol{\Pi}\cdot\mathbf{P}_1\right) + \frac{1}{4\pi}\widehat{\mathbf{R}}\times\mathbf{F}^c\right]. \quad (B2)$$

The force balances of Eqs. (48) and (49) are also modified as

$$\mathbf{U}_1 = -\frac{1}{R^2}\boldsymbol{\Omega}_2\times\widehat{\mathbf{R}} + \frac{1}{3\pi\,\mathrm{Ma}}(\mathbf{F}_1+\mathbf{F}^c), \quad (B3)$$

$$\mathbf{U}_2 = \frac{1}{R^2}\boldsymbol{\Omega}_1\times\widehat{\mathbf{R}} + \frac{1}{3\pi\,\mathrm{Ma}}(\mathbf{F}_2-\mathbf{F}^c). \quad (B4)$$

To determine the contact force, we prescribe that there be rolling without slipping between the two touching surfaces, which is expressed as

$$\mathbf{U}_1 + \boldsymbol{\Omega}_1\times\widehat{\mathbf{R}} = \mathbf{U}_2 - \boldsymbol{\Omega}_2\times\widehat{\mathbf{R}}. \quad (B5)$$

If $\mathbf{P}_1$ and $\mathbf{P}_2$ are known, Eqs. (B1)–(B5) form a system of five vector equations for the five unknowns $\boldsymbol{\Omega}_1$, $\boldsymbol{\Omega}_2$, $\mathbf{U}_1$, $\mathbf{U}_2$, and $\mathbf{F}^c$. This system can be inverted analytically, yielding new expressions for $\boldsymbol{\Omega}_1$, $\boldsymbol{\Omega}_2$, $\mathbf{U}_1$, and $\mathbf{U}_2$ to be used instead of Eqs. (54)–(57) when the two particles are in contact.

[1] A. P. Gast and C. F. Zukoski, Adv. Colloid Interface Sci. **30**, 153 (1989).

[2] T. C. Halsey, Science **258**, 761 (1992).

[3] M. Parthasarathy and D. J. Klingenberg, Mater. Sci. Eng. **17**, 57 (1996).

[4] P. Sheng and W. Wen, Annu. Rev. Fluid Mech. **44**, 143 (2012).

[5] X. Niu, W. Wen, and Y. Lee, Appl. Phys. Lett. **87**, 243501 (2005).

[6] K. Shimada and T. Fujita, Exp. Mech. **40**, 231 (2000).

[7] R. Stanway, J. L. Sproston, and A. K. El-Wahed, Smart Mater. Struct. **5**, 464 (1996).

[8] K. Yoshida, M. Kikuchi, J. Park, and S. Yokota, Sens. Actuators A **95**, 227 (2002).

[9] X. Niu, L. Liu, W. Wen, and P. Sheng, Phys. Rev. Lett. **97**, 044501 (2006).

[10] L. Wang, M. Zhang, J. Li, X. Gong, and W. Wen, Lab Chip **10**, 2869 (2010).

[11] T. C. Halsey and W. Toor, Phys. Rev. Lett. **65**, 2820 (1990).

[12] A. Kumar, B. Khusid, Z. Y. Qiu, and A. Acrivos, Phys. Rev. Lett. **95**, 258301 (2005).

[13] J. S. Park and D. Saintillan, Phys. Rev. E **83**, 041409 (2011).

[14] J. S. Park and D. Saintillan, Soft Matter **7**, 10720 (2011).

[15] C. Boissy, P. Atten, and J.-N. Foulc, J. Electrost. **35**, 13 (1995).

[16] W. Weiler, Z. Phys. Chem. Unterricht **4**, 194 (1893).

[17] G. Quincke, Ann. Phys. Chem. **59**, 417 (1896).

[18] A. O. Cebers, Mekh. Zhidk. Gaza **2**, 86 (1980).

[19] T. B. Jones, IEEE Trans. Ind. Appl. **IA-20**, 845 (1984).

[20] J. R. Melcher and G. I. Taylor, Annu. Rev. Fluid Mech. **1**, 111 (1969).

[21] D. A. Saville, Annu. Rev. Fluid Mech. **29**, 27 (1997).

[22] E. N. Lorenz, J. Atmos. Sci. **20**, 130 (1963).

[23] E. Lemaire and L. Lobry, Physica A **314**, 663 (2002).

[24] F. Peters, L. Lobry, and E. Lemaire, Chaos **15**, 013102 (2005).

[25] S. Krause and P. Chandratreya, J. Colloid Interface Sci. **206**, 10 (1998).

[26] J.-W. Ha and S.-M. Yang, Phys. Fluids **12**, 764 (2000).

[27] P. F. Salipante and P. M. Vlahovska, Phys. Fluids **22**, 112110 (2010).

[28] H. He, P. F. Salipante, and P. M. Vlahovska, Phys. Fluids **25**, 032106 (2013).

[29] L. Lobry and E. Lemaire, J. Electrost. **47**, 61 (1999).

[30] E. Lemaire, L. Lobry, and N. Pannacci, J. Electrost. **64**, 586 (2006).

[31] N. Pannacci, E. Lemaire, and L. Lobry, Rheol. Acta **46**, 899 (2007).

[32] E. Lemaire, L. Lobry, N. Pannacci, and F. Peters, J. Rheol. **52**, 769 (2008).

[33] F. Peters, L. Lobry, and E. Lemaire, J. Rheol. **54**, 311 (2010).

[34] H.-F. Huang, M. Zahn, and E. Lemaire, J. Electrost. **68**, 345 (2010).

[35] H.-F. Huang, M. Zahn, and E. Lemaire, J. Electrost. **69**, 442 (2011).

[36] H. Brenner, J. Colloid Interface Sci. **32**, 141 (1970).

[37] L. Jibuti, S. Rafaï, and P. Peyla, J. Fluid Mech. **693**, 345 (2012).

[38] A. Cebers, E. Lemaire, and L. Lobry, Magnetohydrodynamics **36**, 347 (2000).

[39] N. Pannacci, L. Lobry, and E. Lemaire, Phys. Rev. Lett. **99**, 094503 (2007).

[40] J. T. K. Wan, K. W. Yu, and G. Q. Gu, Phys. Rev. E **62**, 6846 (2000).

[41] Y. Dolinsky and T. Elperin, Phys. Rev. E **85**, 026608 (2012).

[42] D. Saintillan, Phys. Fluids **20**, 067104 (2008).

[43] J. D. Jackson, *Classical Electrodynamics* (Wiley, New York, 1962).

[44] J. G. Méndez-Bermúdez and I. Santamaría-Holek, Physica A **389**, 1819 (2010).

[45] H. Híjar, J. G. Méndez-Bermúdez, and I. Santamaría-Holek, J. Chem. Phys. **132**, 084502 (2010).

[46] T. B. Jones and M. Washizu, J. Electrost. **37**, 121 (1996).

[47] S. Kim and S. P. Karrila, *Microhydrodynamics: Principles and Selected Applications* (Butterworth-Heinemann, Oxford, 1991).

[48] M. Washizu, J. Electrost. **29**, 177 (1992).

[49] See Supplemental Material at http://link.aps.org/supplemental/10.1103/PhysRevE.87.043014 for a movie showing the dynamics in cases 1 through 4 of Fig. 11.

[50] J. S. Park and D. Saintillan, J. Fluid Mech. **662**, 66 (2010).